RAPID COMMUNICATIONS

PHYSICAL REVIEW B VOLUME 38, NUMBER 11 15 OCTOBER 1988-I

Evidence of a mobility edge in the second subband of an $Al_{0.33}Ga_{0.67}As$-GaAs heterojunction

R. Fletcher and E. Zaremba
Department of Physics, Queen's University, Kingston, Ontario, Canada K7L 3N6

M. D'Iorio
Division of Physics, National Research Council of Canada, Ottawa, Ontario, Canada K1A OR6

C. T. Foxon and J. J. Harris
Philips Research Laboratories, Redhill, Surrey, England RH1 5HA

(Received 1 April 1988)

We report on simultaneous measurements of mobility and Dingle temperature of a two-dimensional electron gas in an AlGaAs/GaAs heterojunction, the density of which is varied by means of infrared illumination. Detailed measurements reveal that the Dingle temperature of the first subband decreases abruptly as a function of density when the second subband becomes occupied but the accompanying drop in mobility occurs smoothly over a broader density interval. We interpret these results as indicating the existence of a mobility edge at the bottom of the second subband.

The effect of strong localization associated with the disorder scattering of electrons in a two-dimensional electron gas (2D EG) has been studied intensively in Si metal-oxide-semiconductor field-effect transistors particularly with regard to the existence of a mobility edge and a minimum metallic conductivity.[1,2] These studies were facilitated by the controlled variability of the 2D EG density whereby the Fermi level could be positioned in the range of either localized or delocalized states. Similar experiments are surprisingly scarce for heterostructures,[3] partly for the reason that interest was diverted to the effects of weak localization[4] which recently has been studied in high-mobility samples.[5,6]

In this paper we present evidence for strong localization in a 2D EG at an AlGaAs/GaAs heterojunction in which two subbands are occupied. One of the unique features of our experiments is that the bottom of the second subband and its mobility edge can be detected by the behavior of the electrons in the first subband. As the Fermi energy E_F enters the range of localized states below the mobility edge, the additional channel for scattering from the first to the second subband influences the mobility even though there are no mobile carriers in the second subband. Subsequently, as E_F passes through the mobility edge, the second subband electrons become available for metallic screening of the impurity potential. Because of the unique screening properties of a 2D EG, the immediate effect is an abrupt increase in the lifetime of the states in the first subband, a feature which can be explored by means of the Shubnikov-de Haas (SdH) oscillations. Other independent information, to be discussed later, is also available to locate the mobility edge. We anticipate that this approach will prove to be a general probe of the mobility edge and its location relative to the bottom of the band.

The sample was fabricated by molecular-beam epitaxy at Philips Research Laboratories and has no intentional undoped spacer layer between the Si-doped $Al_{0.33}Ga_{0.67}As$ and GaAs layers. The total carrier density could be incrementally increased from $5\times10^{15}\ m^{-2}$ to $10\times10^{15}\ m^{-2}$ using radiation from an infrared light-emitting diode filtered by a wafer of GaAs to prevent the generation of electron-hole pairs. Under these conditions the extra carriers are known to originate from ionization of *DX* centers in the AlGaAs, and the depletion layer in the GaAs remains undisturbed.[7,8] Different cooling times yielded slightly different starting values for the initial properties, but all qualitative features are reproducible.

At each increment of electron density, various types of experimental data were taken. The Hall resistivity ρ_{xy}, equal to B/en_T in the magnetic field range $B=0.2$–1.4 T, provided accurate values of the total density n_T of delocalized electrons. Measurement of the zero-field resistivity ρ_{xx} then yields the average transport mobility $\langle\mu\rangle$ as shown in Fig. 1(c). The decrease in the mobility in the density range 6.7 to $7.5\times10^{15}\ m^{-2}$ is due to the onset of intersubband scattering and a reduction of the first subband transport lifetime.[9,10]

The calculated mobility is shown in Fig. 2(c) and is in qualitative agreement with the experimental results. The Boltzmann transport calculations are based on a two-band model in which disorder broadening of the density of states is neglected; the band edge is then characterized by a discontinuous change in density of states of $m^*/\pi\hbar^2$. The subband mobilities μ_i are given by $e\tau_i/m^*$, where the transport relaxation time τ_i for the ith subband is determined by the equation

$$\sum_{j=1,2} K_{ij}(E_F)\tau_j(E_F) = E_F - E_i. \quad (1)$$

The interband scattering matrix $K_{ij}(E_F)$ is defined[2,11] in terms of the configuration-averaged square of the impurity scattering matrix element, $|V_{ij}(\mathbf{q})|^2$. We assume that the scattering is due to the linearly screened electrostatic potential of the ionized donors in the AlGaAs which are

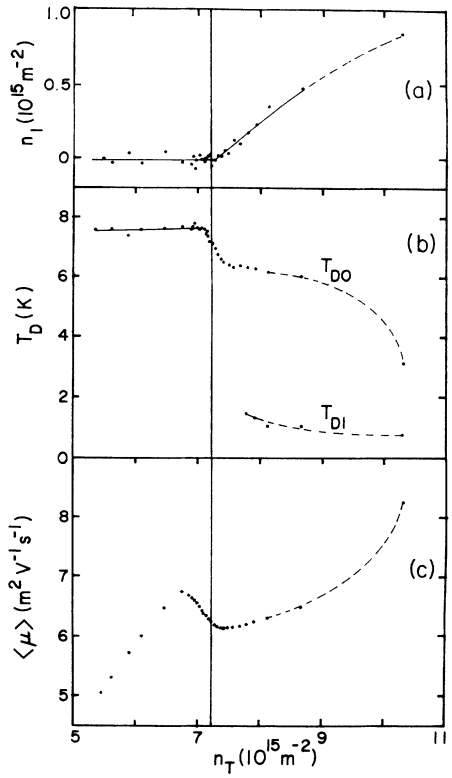

FIG. 1. (a) Second subband density $n_1 = n_T - n_0$ vs total density n_T. (b) Dingle temperatures of the first T_{D0} and second T_{D1} subbands as a function of n_T. (c) Average mobility vs n_T. The vertical line at $n_T = 7.2\times10^{15}$ m^{-2} denotes the first observation of second subband occupancy in ρ_{xx}. The lines through the data points are simply a guide to the eye.

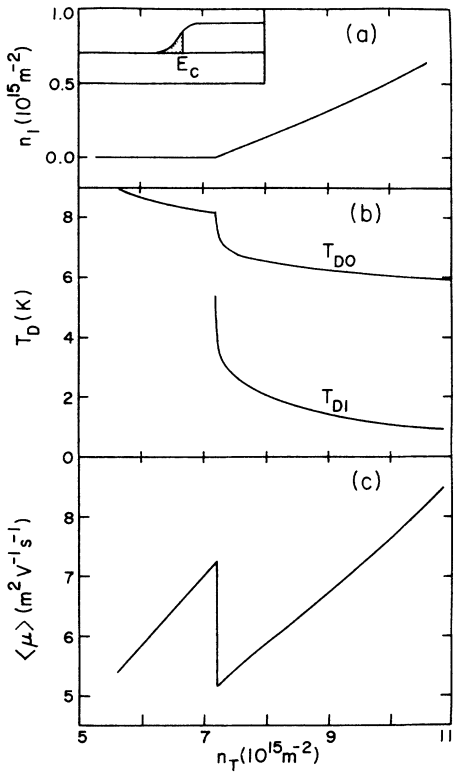

FIG. 2. (a)–(c): As in Fig. 1, but theory. Parameters used in the calculations are Si-doping density equal to 1.3×10^{24} m^{-3}, donor density $n_d = 5.96\times10^{15}$ m^{-2}, doping density (GaAs) equal to 1.0×10^{20} m^{-3}, depletion density equal to 0.46×10^{15} m^{-2}, undoped spacer width $s = 15$ Å (an unintentional spacer of about 10 Å is expected). (a) is the second subband density vs total density, according to Eq. (4); the inset is a qualitative sketch of the impurity broadened second subband density of states with a mobility edge at E_C.

confined within a width w separated from the interface by an undoped spacer of width s; scattering due to ionized acceptors in the GaAs was found to be unimportant. In this situation the scattering matrix element is given by

$$|V_{ij}(\mathbf{q})|^2 = n_d f(q)\left|\frac{2\pi e^2}{\kappa q}\sum_{kl}(\epsilon^{-1})_{ij,kl}V_{kl}^{\mathrm{ext}}(q)\right|^2, \qquad (2)$$

where n_d is the ionized donor areal density,

$$f(q) = (1-e^{-2qw})e^{-2qs}/2qw$$

is the impurity form factor, and $\epsilon_{ij,kl}$ is the intersubband dielectric matrix.[2] $V_{ij}^{\mathrm{ext}}(q)$ is the bare Coulomb impurity matrix element. The other symbols have their usual significance.

Analytic subband wave functions of the form[9] $\phi_0(z) = 2\alpha^{3/2}ze^{-\alpha z}$ for the first subband, and

$$\phi_1(z) = 2\sqrt{3}\beta^{5/2}(\alpha^2-\alpha\beta+\beta^2)^{-1/2}z[1-\tfrac{1}{3}(\alpha+\beta)z]e^{-\beta z}$$

for the second subband, were used in the calculations. The exponents α and β in the density range of interest were obtained from a comparison with self-consistent calculations of the electronic density.[12] The assumption that the photogenerated charge centers in the AlGaAs are remote and contribute only to the average interface electric field but not to the disorder potential leads to a mobility which is in better agreement with experiment, both in magnitude and general density dependence, when experimentally defined values for the various impurity parameters are used. This supports the overall scenario for photogeneration[7,8] and the assumption that the ionized donors provide the dominant scattering mechanism.

The sharp step in the calculated mobility is of course a consequence of the assumed steplike increase in the second subband density of states and contrasts with the smooth transition seen in Fig. 1(c). As indicated in the inset to Fig. 2(a), the random impurity potential is expected to broaden the band edge and to give rise to a decaying low-energy tail in the density of states. In this situation the sharp discontinuity in the calculated mobility will be smeared out[9] and the change will appear less prominent.

At each electron density we have also examined the SdH oscillations in ρ_{xx} over the magnetic field range $0 < B < 2.2$ T. The oscillatory part $\tilde{\rho}_{xx}$ is assumed to be described by [13]

$$\tilde{\rho}_{xx} = \sum_i C_i(X/\sinh X)\exp(-2\pi^2kT_{D_i}/\hbar\omega_c) \times\cos\left(\frac{2\pi f_i}{B}+\phi\right), \qquad (3)$$

where $X=2\pi^2kT/\hbar\omega_c$, T_{D_i} is the Dingle temperature of the ith subband, $f_i=n_ih/2e$ is its frequency, and the amplitude C_i is discussed below. When only the lower subband is occupied, the electron densities, say n_0, obtained from the single frequency f_0, agree with those obtained from ρ_{xy} to an accuracy of $\simeq 0.5\%$. This suggests that inhomogeneities in the sample are unimportant because ρ_{xx} is determined by a much larger area of the sample than is ρ_{xy}.

In the region of $n_T=7\times10^{15}$ m^{-2} the second subband becomes occupied and makes itself evident in three ways: a second SdH oscillation frequency appears, the Dingle temperature of the first subband oscillation is reduced, and n_T and n_0 are no longer the same. The difference n_T-n_0 is taken to be n_1, the density in the second subband, and this is shown in Fig. 1(a). The point at which a second oscillation is first visible in ρ_{xx} is indicated by the vertical line at $n_T=7.2\times10^{15}$ m^{-2} in Fig. 1. We recognize its appearance by an initial rise in ρ_{xx} versus magnetic field; with a single band present, ρ_{xx} always initially decreases with B. Finally, we fit the envelope function of the oscillations appropriate to both n_0 and n_1 using the prefactor to the oscillating term of Eq. (3). We have done this using both $C_i=$const (Ref. 13) or by including an extra factor[14] within C_i of $(\omega_c\tau_{D_i})^2/[1+(\omega_c\tau_{D_i})^2]$ where $\tau_{D_i}^{-1}=2\pi kT_{D_i}/\hbar$. The quality of the fits is marginally better using the simple constant but the difference is too small to be significant. However, the values of T_D obtained by the two methods are different, with the latter being consistently about 30% smaller than the former, but otherwise sharing identical structure. We have chosen to present the former data, and this is shown in Fig. 1(b) for both subbands. When the second subband is not occupied, the Dingle temperature of the first subband T_{D0} shows little variation with n_0. At the point at which n_1 first becomes finite (as indicated by the presence of the second SdH oscillation) T_{D0} begins to drop rapidly but appears to level off to a new value with increasing n_T (before finally decreasing again in a way that is not understood).

The Dingle temperature, which is a measure of the lifetime broadening, has been estimated from the total single-particle scattering rate induced by the screened impurity potential, and the results are shown in Fig. 2(b). At first sight one might guess that the increased scattering rate associated with intersubband transitions would increase T_{D0}. In fact, intersubband scattering plays a relatively minor role and the main effect is due to the additional screening of the impurity potential provided by the electrons in the second subband. The single-particle lifetime is influenced by scattering in the full range of momentum transfers $0\rightarrow 2k_{F0}$, and in particular is dominated by small-q or small-angle scattering where the scattering potential is strongest. Delocalized electrons in the second subband effectively screen all Fourier components of the potential up to $2k_{F1}$, and as a result the scattering potential is weakened and the lifetime of the first subband electrons increases more than enough to compensate for interband scattering. The same calculations also predict that the second subband has a much lower Dingle temperature T_{D1} than the first, a result consistent with the experimental observations in Fig. 1(b).

It will be seen from Fig. 1 that all data obtained from SdH oscillations are self-consistent and indicate essentially a single density n_T at which n_1 appears (i.e., the abrupt drop of T_{D0}, the departure of $n_1=n_T-n_0$ from zero, and the visible occurrence of second band occupancy in ρ_{xx}). Nevertheless $\langle\mu\rangle$ shows the presence of the second subband before any of the above. The different behavior is incompatible with sample inhomogeneity or finite-temperature broadening, but can be explained in terms of a mobility edge near the bottom of the second subband. As the Fermi level enters the tail of the second subband density of states, intersubband scattering turns on gradually with transitions into localized states and leads to a relatively gently drop in $\langle\mu\rangle$. Only with the appearance of delocalized states above the mobility edge does metallic screening of the impurity potential become effective, leading to the abrupt drop in T_{D0}. The absolute magnitude of the energy broadening at the bottom of the second subband, ΔE_1, can be inferred from the width in n_T of the mobility transition and is about 10–20 K. This is consistent with the observed Dingle temperature. The finite temperature of 1.17 K used in the experiments will lead to some broadening and may be responsible for the slight rounding of the T_{D0}-versus-n_T curve noticeable in Fig. 1(b) just before the abrupt drop.

Another feature that might not be expected immediately is the rather slow rate of increase of n_1 with n_T, which for a fixed intersubband energy separation is $dn_1/dn_T=0.5$. A partial explanation of the difference is based on the fact that an important part of the density variation of the mobility arises from the density dependence of the subband wave function. The exponent α is mainly governed by the interface electric field $\mathcal{E}$ which is approximately $2\pi en_T/\kappa$ when the depletion density in the GaAs is small. For a model triangular potential, the exponent α is proportional to $\mathcal{E}^{1/3}$ or $n_T^{1/3}$. In this picture the energy separation E_1-E_0 is proportional to $n_T^{2/3}$ and the increasing separation with density inhibits the population of the second subband. Defining the critical density $n_T=n_C$ at which the second subband first becomes populated, the second subband density is given by

$$n_1=\tfrac{1}{2}n_T\left[1-\left(\frac{n_C}{n_T}\right)^{1/3}\right], \tag{4}$$

which reduces to $\frac{1}{6}(n_T-n_C)$ for small deviations from n_C. Equations (4) is plotted in Fig. 2(a); it represents the results of the self-consistent calculations[11] very well but underestimates somewhat the observed magnitude of the second subband density. We conjecture that this may be due to the release of localized carriers in both the first and second subbands as the screening of the impurity potential is enhanced with the second subband occupancy. This is a detail which should be explored more thoroughly.

In summary, the present data reveal many interesting features. Most of these are quantitatively described by the calculation, i.e., the magnitude of the mobility and its decrease with intersubband scattering, the drop of T_{D0} at the point at which delocalized electrons appear in the second subband as well as the much lower Dingle temperature of the second subband. All of these observations are

consistent with disorder broadening of the second subband and the existence of a mobility edge, and the present techniques allow detailed investigation of these interesting strong localization phenomena.

The authors wish to thank Dr. F. Stern for providing the results of self-consistent quantum-well calculations. Financial support of the Natural Sciences and Engineering Research Council of Canada is gratefully acknowledged.

[1]M. Pepper, Proc. Soc. London, Ser. A **353**, 225 (1977).

[2]T. Ando, A. B. Fowler, and F. Stern, Rev. Mod. Phys. **54**, 437 (1982).

[3]C. T. Foxon, J. J. Harris, R. G. Wheeler, and D. E. Lacklison, J. Vac. Sci. Technol. B **4**, 511 (1986).

[4]P. A. Lee and T. V. Ramakrishnan, Rev. Mod. Phys. **57**, 287 (1985).

[5]B. J. F. Lin, M. A. Paalanen, A. C. Gossard, and D. C. Tsui, Phys. Rev. B **29**, 927 (1984).

[6]K. K. Choi, D. C. Tsui, and S. C. Palmateer, Phys. Rev. B **33**, 8216 (1986).

[7]A. Kastalsky and J. C. M. Hwang, Solid State Commun. **51**, 317 (1984).

[8]J. J. Harris, D. E. Lacklison, C. T. Foxon, F. M. Selton, A. M. Suckling, R. J. Nicholas, and K. W. J. Barnham, Semicond. Sci. Technol. **2**, 783 (1987).

[9]S. Mori and T. Ando, Phys. Rev. B **19**, 6433 (1979); D. G. Cantrell and P. N. Butcher, J. Phys. C **18**, 5111 (1985).

[10]H. L. Störmer, A. C. Gossard, and W. Wiegmann, Solid State Commun. **41**, 707 (1982).

[11]E. D. Siggia and P. C. Kwok, Phys. Rev. B **2**, 1024 (1970).

[12]F. Stern and S. Das Sarma, Phys. Rev. B **30**, 840 (1984); F. Stern (private communication).

[13]T. Ando, J. Phys. Soc. Jpn. **37**, 1233 (1974); T. Ando, Y. Matsumoto, and Y. Uemura, *ibid.* **39**, 279 (1975).

[14]A. D. C. Grassie, K. M. Hutchings, M. Lakrimi, C. T. Foxon, and J. J. Harris, Phys. Rev. B **36**, 4551 (1987).

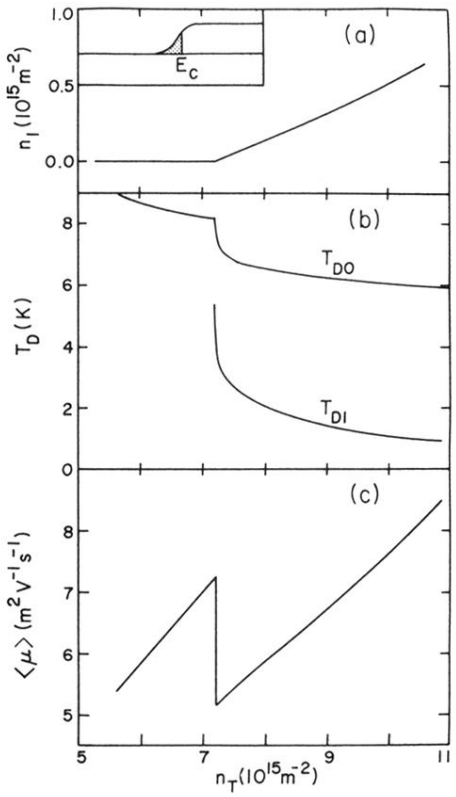

FIG. 2. (a)–(c): As in Fig. 1, but theory. Parameters used in the calculations are Si-doping density equal to 1.3×10^{24} m^{-3}, donor density $n_d = 5.96\times10^{15}$ m^{-2}, doping density (GaAs) equal to 1.0×10^{20} m^{-3}, depletion density equal to 0.46×10^{15} m^{-2}, undoped spacer width $s = 15$ Å (an unintentional spacer of about 10 Å is expected). (a) is the second subband density vs total density, according to Eq. (4); the inset is a qualitative sketch of the impurity broadened second subband density of states with a mobility edge at E_C.